


First in-human PET study and kinetic evaluation of [¹⁸F]AS2471907 for imaging 11 β -hydroxysteroid dehydrogenase type I

Shivani Bhatt^{1,2} , Nabeel B Nabulsi², Songye Li², Zhengxin Cai², David Matuskey^{2,3}, Jason Bini², Soheila Najafzadeh², Michael Kapinos², Jim R Ropchan², Richard E Carson², Kelly P Cosgrove^{1,2,3,4}, Yiyun Huang² and Ansel T Hillmer^{2,3}

Abstract

11 β -Hydroxysteroid dehydrogenase type I (11 β -HSDI) catalyzes enzymatic conversion of cortisone into the stress hormone cortisol. This first-in-human brain imaging study characterizes the kinetic modeling and test–retest reproducibility of [¹⁸F]AS2471907, a novel PET radiotracer for 11 β -HSDI. Eight individuals underwent one 180-min ($n = 4$) or two 240-min ($n = 4$) [¹⁸F]AS2471907 PET brain scans (12 total) acquired on the high-resolution research tomograph (HRRT) scanner with arterial blood sampling. Imaging data were modeled with 1-tissue (1T) and 2-tissue (2T) compartment models and with multilinear analysis (MAI) to estimate [¹⁸F]AS2471907 availability (V_T). [¹⁸F]AS2471907 demonstrated high, heterogeneous uptake throughout the brain. Of the compartment models, 2T best described [¹⁸F]AS2471907 data. Estimates of V_T were highly correlated between 2T and MAI ($t^* = 30$ min) with MAI yielding V_T values ranging from 3.2 ± 1.0 mL/cm³ in the caudate to 15.7 ± 4.2 mL/cm³ in the occipital cortex. The median absolute test–retest variability of $16 \pm 5\%$ and high intraclass correlation coefficient (ICC) values of 0.67–0.97 across regions indicate fair test–retest reliability but large intersubject variability. V_T estimates using 180 min were within 10% of estimates using full acquisition time. In summary, [¹⁸F]AS2471907 exhibits reasonable kinetic properties for imaging 11 β -HSDI in human brain.

Keywords

Molecular imaging, neurochemistry, positron emission tomography, steroids, stress/chronic stress

Received 18 December 2018; Revised 8 February 2019; Accepted 11 February 2019

Introduction

Cortisol is a steroid hormone that binds to glucocorticoid and mineralocorticoid receptors (GR and MR) throughout the body, affecting the regulation of metabolism and blood pressure. In the brain, cortisol regulates a canonical neuroendocrine stress pathway, the hypothalamic-pituitary-adrenal (HPA) axis. Cortisol binding to GRs in the cortical and limbic regions of the brain produces negative feedback onto the HPA axis and suppresses downstream peripheral cortisol release.¹ Dysregulation of peripheral cortisol levels has been observed in a number of conditions including depression,² post-traumatic stress disorder,^{3,4} and obesity.^{5,6}

¹Interdepartmental Neuroscience Program, Yale University School of Medicine, New Haven, CT, USA

²Yale PET Center, Department of Radiology and Biomedical Imaging, Yale University School of Medicine, New Haven, CT, USA

³Department of Psychiatry, Yale University School of Medicine, New Haven, CT, USA

⁴National Center for PTSD, West Haven VA Hospital, West Haven, CT, USA

Corresponding author:

Ansel T Hillmer, Departments of Radiology and Biomedical Imaging and Psychiatry, Yale University School of Medicine, 2 Church St S Suite 314, New Haven, CT 06511, USA.
Email: ansel.hillmer@yale.edu

11 β -Hydroxysteroid dehydrogenase type 1 (11 β -HSD1) is an intracellular enzyme that catalyzes the interconversion of the steroid hormones cortisone and cortisol. The enzyme's bidirectional function in vitro becomes unidirectional in the reductive environment generated by abundant NADPH in most intact cells: in vivo, 11 β -HSD1 primarily catalyzes the forward conversion of cortisone into cortisol, while the reverse direction is catalyzed by 11 β -HSD2.⁷ Cortisol produced in the adrenal cortex as an end product of the steroidogenesis cascade is known to contribute to cortisol in the brain.⁸ However, efflux of cortisol from the brain mediated by p-glycoprotein suggests that an additional brain-specific source of cortisol contributes to brain glucocorticoid signaling.⁸ The exclusive expression of 11 β -HSD1 in brain⁷ implicates it as an important brain-specific source of cortisol. This functionality suggests a critical role of 11 β -HSD1 in regulating cortisol-mediated negative feedback onto the HPA axis. Indeed, preclinical studies have reported enhanced spatial memory and stress resilience in mice with *HSD11b1* gene deletion,^{9,10} and reduction in contextual fear-conditioning with systemic administration of an 11 β -HSD1 inhibitor.¹¹ These findings motivate 11 β -HSD1 as a potential target for pharmacological intervention in neuropsychiatric, metabolic, and inflammatory conditions.^{12–14}

PET radioligands with specificity for 11 β -HSD1 would provide highly useful tools to study the glucocorticoid system in vivo. We previously reported the development of [¹¹C]AS2471907 (Figure 1), a radiolabeled inhibitor of 11 β -HSD1, and characterization of its kinetics in human brain.¹⁵ However, the radiochemical yield was low and inconsistent, as the desired compound [¹¹C]AS2471907 was produced as a minor product in the radiosynthetic process due to the formation of two undesired regio-isomers.¹⁵ Thus, our group developed an F-18 analog, [¹⁸F]AS2471907 (Figure 1),¹⁶ with the goals of increasing the radiochemical yield and improving the quantification properties from higher counting statistics afforded by the longer-lived fluorine-18 radiolabel. The aim of this work is to describe the first in-human brain imaging with

[¹⁸F]AS2471907 PET and to characterize the optimal imaging and kinetic modeling approaches for this novel radiotracer.

Methods

Research participants

Eight healthy individuals participated in the study (2 women, 6 men; age = 30.0 \pm 4.1 years; BMI = 25.8 \pm 3.8). Written informed consent was obtained from all participants after a complete explanation of study procedures. All participants were evaluated with medical and psychiatric histories, physical examination, neurological and mental status exam, routine laboratory studies and electrocardiogram, and screened with the Structured Clinical Interview for the DSM-IV or DSM-5 to confirm no current medical or primary psychiatric diagnoses. Participants were not currently taking any medication, including psychoactive medication. All procedures were approved and overseen by the Yale University Institutional Human Investigation Committee and the Yale New Haven Hospital Radiation Safety Committee, and in accordance with Code of Federal Regulations Title 45, Part 46 policy on protection of human subjects in research.

Radiotracer synthesis

The novel radiotracer [¹⁸F]AS2471907 was prepared according to previously published procedures.¹⁶

Image acquisition

Four participants underwent both a test and retest PET scan one to two weeks apart from each other (1 woman, 3 men; age = 31.8 \pm 5.6 years), and four had a single PET scan (1 woman, 3 men; age = 28.3 \pm 1.0 years). Test and retest scans were 240 min in length with a 30-min break at 120 min, while single scans were 180 min in length with a 30-min break at 90 min. Injection time was carefully controlled to be between 11:00 a.m. and 1:30 p.m. for all participants, to minimize effects of possible variation in 11 β -HSD1 availability associated with known diurnal fluctuations in cortisol.¹⁷ [¹⁸F]AS2471907 was injected in an antecubital vein of the dominant arm as a 1-min bolus using an automated infusion pump (Harvard PHD 22/2000; Harvard Apparatus, Holliston, MA, USA). PET data were acquired in list-mode on the High-Resolution Research Tomograph (HRRT; Siemens, Medical Solutions, Knoxville, TN, USA). Head motion data were acquired with a frequency of 20 Hz with the Polaris Vicra optical tracking system (NDI Systems, Waterloo, Canada). List-mode data were reconstructed

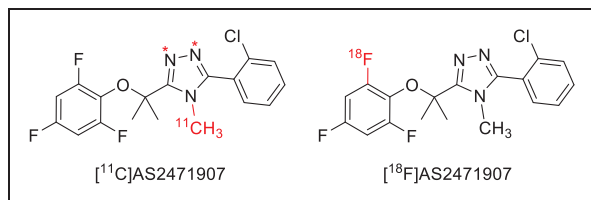


Figure 1. Structure of PET radiotracers [¹¹C]AS2471907 (with * indicating the labeling positions of regioisomers) and [¹⁸F]AS2471907.

using the MOLAR algorithm¹⁸ into histogrammed time bins (6×0.5 min, 3×1 min, 2×2 min, 5 min to scan end) with corrections for subject motion, attenuation, scatter, randoms, and dead time.

Blood analysis

For each scan, an arterial line was placed in the radial artery contralateral to radiotracer injection site for blood sampling to measure radioactivity concentration and radioactive metabolites in plasma. Plasma samples were acquired every 10 s for 3 min immediately following radiotracer injection and then at 5, 10, 20, 30, 45, 60, 75, 90, 105, 120, 150, 180, 210, and 240 min post-injection. Whole blood and plasma radioactivity were measured by cross-calibrated gamma counter (1480 Wizard, Perkin-Elmer, Waltham, MA, USA). Plasma was obtained by centrifugation at 4°C at 2930g for 5 min. Assayed radioactivity for each sample was decay-corrected to time of radiotracer injection. The plasma radioactivity curve was fit with a sum of exponentials function.

Metabolite analysis was performed on plasma samples from 10, 30, 60, 90, 120, 180, and 240 min using an automated column-switching HPLC system.¹⁹ Flow rate for the mobile phase (45% 50 mM ammonium acetate, 55% acetonitrile) was optimized to elute parent [¹⁸F]AS2471907 off the analytical column (Phenomenex Luna 5u Phenyl-Hexyl; 250 × 4.6mm, 5 μm) between 10 and 12 min. Fraction-collected radioactivity corresponding to the parent peak was integrated and normalized to total eluted radioactivity to determine parent fraction. The parent fraction measurements as a function of time were fitted with an inverse gamma function.

Arterial input functions were calculated as the product of plasma radioactivity concentration and normalized parent fraction fitted curve. Free fraction in plasma (f_p) was measured in triplicate with ultrafiltration (Millipore Centrifree micropartition device 4104, Billerica, MA, USA) according to manufacturer guidelines with 4 mL of pre-injection arterial blood. Values of f_p were calculated as the ratio of radioactivity in ultrafiltrate to total radioactivity in plasma.

Image processing

A high-resolution T1-weighted structural MRI was acquired for each participant for co-registration of PET to MR image. Structural MRI images were acquired with a sagittal gradient-echo (MPRAGE) sequence (Siemens 3.0T Prisma Fit; 176 sagittal slices, thickness = 1 mm, TR = 2530 ms, TE = 2.26 ms, flip angle = 7°, FoV = 256 mm, matrix size = 256 × 256, $1 \times 1 \times 1$ mm³ voxels). A PET image summed from

0 to 10 min was co-registered with a rigid-body transform to the individual participant's MRI, which was in turn normalized with a nonlinear registration into a template space (Montreal Neurological Institute). All subsequent frames were aligned using rigid-body transform to the co-registered 0–10 min sum PET image. Automatic anatomical labeling (AAL)-defined regions of interests (ROIs) on MRI were transformed and applied to PET images in PET space to determine time-activity curves within ROIs.²⁰ AAL-defined ROIs were the amygdala, caudate, cerebellum, anterior cingulum, frontal cortex, hippocampus, insula, occipital cortex, parietal cortex, putamen, temporal cortex, thalamus (all with gray matter masking), and the centrum semiovale, a white matter region, in addition to a whole brain ROI.

Kinetic analysis

The primary outcome measure of kinetic analysis was the [¹⁸F]AS2471907 volume of distribution (V_T), which is the ratio of radioactivity concentration in tissue to that in plasma at equilibrium.²¹ A pharmacokinetic modeling approach was used to estimate V_T . Standard 1-tissue (1T) and 2-tissue (2T) compartment models²² were among the model configurations compared to determine the optimal modeling approach. Each compartment model featured either a fixed blood volume fraction (F_V) of 5% based on literature values²³ or an F_V parameter estimated independently for each region. A global time delay factor was incorporated to account for the difference in radiotracer arrival in arterial blood compared to brain tissue.²⁴ Model fits were compared both visually and statistically using Akaike information criteria (AIC) as below, where N is the number of fitted frames, $SumSQ$ is the sum of the squared residuals, and k is the number of model parameters

$$AIC = N \times \ln(SumSQ/N) + 2 \times k$$

For some 2T model fits, a large relative standard error of estimate was observed for V_T and other parameters, indicating an unstable or non-converging model fit. Therefore, multilinear analysis (MA1) with t^* of 15, 30, and 45 min was also used to estimate V_T .²⁵ Optimal t^* time for MA1 was determined to be the t^* that provided the best combination of visual and quantitative fit, as assessed by reduced chi-square estimates, to regional TACs and test-retest reproducibility of V_T .

To determine optimal acquisition duration, time stability of V_T values was evaluated. For the eight test-retest scans (240 min long), V_T was estimated with 120, 150, 180, and 210 min of acquisition data

and normalized to V_T estimated with full acquisition duration of 240 min. Sufficient acquisition duration was determined as the shortest scan time at which normalized V_T values averaged across subjects were 90–110%. Inter-individual standard deviations of normalized V_T values were estimated for all regions.

Reproducibility of outcome parameter estimate V_T was evaluated by calculating test–retest variability (TRV) and absolute TRV ($aTRV$) for four participants as follows (parameters represented by X)

$$TRV = \frac{X_{test} - X_{retest}}{\frac{1}{2}(X_{test} + X_{retest})} \times 100\%$$

$$aTRV = \frac{|X_{test} - X_{retest}|}{\frac{1}{2}(X_{test} + X_{retest})} \times 100\%$$

Reproducibility was also estimated by intraclass correlation coefficient (ICC), which compares between-subject variability, measured using between-subject mean sum of squares ($BSMSS$), to within-subject variability, measured by within-subject mean sum of squares ($WSMSS$) as in the equation below

$$ICC = \frac{BSMSS - WSMSS}{BSMSS + WSMSS}$$

ICC values can range from -1 indicating no reliability to 1 indicating perfect reliability.

To visually assess [^{18}F]AS2471907 V_T throughout the brain, voxel-wise parametric V_T images were generated by applying both the 1T model with an F_V parameter fixed to 5% and MA1 with $t^* = 30$ min to 180 min of data smoothed with a 7 mm Gaussian kernel.

The evaluation of standardized uptake value (SUV) as a semi-quantitative imaging measure was assessed by Pearson's correlations of V_T estimated by MA1 ($t^* = 30$ min) applied to 180 min of data with SUV values averaged across multiple 30-min periods of imaging acquisition (six frames per 30-min period): 60–90 min, 90–120 min, 120–150 min, 150–180 min, 180–210 min, and 210–240 min.

Peripheral cortisol analysis

To examine whether inter-individual differences in cortisol may be associated with [^{18}F]AS2471907 V_T , concentration of plasma cortisol was measured on scan day from blood samples taken 30–60 min before [^{18}F]AS2471907 injection, and subsequently at 0, 30, 60, and 90 min post-injection. From these measurements, two cortisol indices were calculated across 0 to 90 min time points: area under the curve (AUC)²⁶ using average cortisol of two time-points multiplied by the intervening time duration for all cortisol

sample times, and slope of cortisol change.^{27,28} Possible relationships of these cortisol indices with whole-brain [^{18}F]AS2471907 V_T were evaluated using Pearson's correlations.

Results

Radiochemistry

[^{18}F]AS2471907 was prepared in $8.3 \pm 5.9\%$ radiochemical yield (decay-corrected) at the end of bombardment (EOB) based on trapped radioactivity ($n = 12$). Radiochemical and chemical purity was $>99\%$, with molar activity (A_m) of 115 ± 67 MBq/nmol at end of synthesis. Total synthesis time was 85 ± 4 min from EOB.

Injection parameters

Participants were administered [^{18}F]AS2471907 as an injected dose of 95 ± 14 MBq and injected mass of 0.73 ± 0.50 μg across scans, with 97 ± 2 MBq and 0.92 ± 0.75 μg for test and 101 ± 4 MBq and 0.85 ± 0.29 μg for retest scans. No adverse or clinically detectable pharmacologic effects were observed in any of the participants, including no significant changes to vital signs or heart rhythm, which were monitored during and after the scan.

Blood analysis

The average fraction of parent radiotracer in plasma is shown for all scans (Figure 2(a)). There were low levels of radiolabeled metabolites. Parent fractions 240 min after radiotracer injection were $66 \pm 21\%$ (test, $n = 4$) and $67 \pm 7\%$ (retest, $n = 4$), with no significant difference in parent fraction across time points between the test and retest scans. Metabolite-corrected input functions were in good agreement between test and retest scans for all participants (Figure 2(b)). Free fraction of the radiotracer in plasma (f_p) was very low, ranging from 0.47% to 0.68%.

Qualitative image analysis

Across subjects, [^{18}F]AS2471907 injection resulted in high uptake throughout the brain, with notably higher uptake in gray matter compared to white matter regions. SUV values peaked at 1.5–2.5 at around 20–30 min in regions of elevated uptake such as occipital cortex, parietal cortex, cerebellum, and thalamus, while peaking at 1.0–1.5 during the first 5 min in regions of moderate to low uptake, such as caudate, anterior cingulum, and hippocampus (Figure 3). This was followed by slow decline over 240 min, consistent with a gradual washout of the radiotracer.

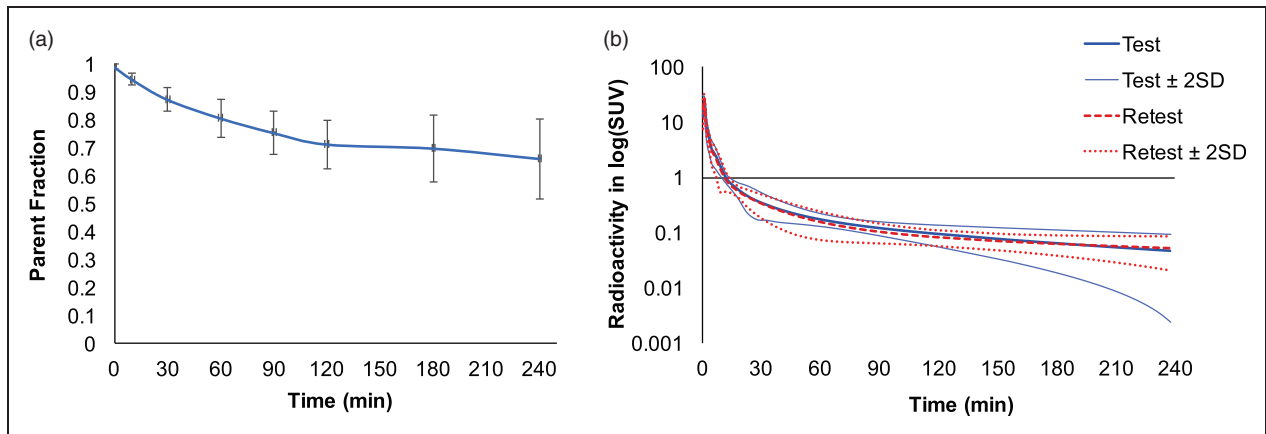


Figure 2. Radiotracer parent fraction and metabolite-corrected arterial input functions. (a) The parent fraction of [^{18}F]AS2471907 measured in plasma. Data are mean \pm SD, with $n = 12$ except at 240-min ($n = 8$). (b) Test (blue solid bold) and retest (red dashed) arterial input functions, with 95% confidence intervals shown for test (blue solid) and retest (red dotted lines), respectively. Data are mean \pm SD with $n = 12$ for 0–180 min and $n = 8$ for 180–240 min.

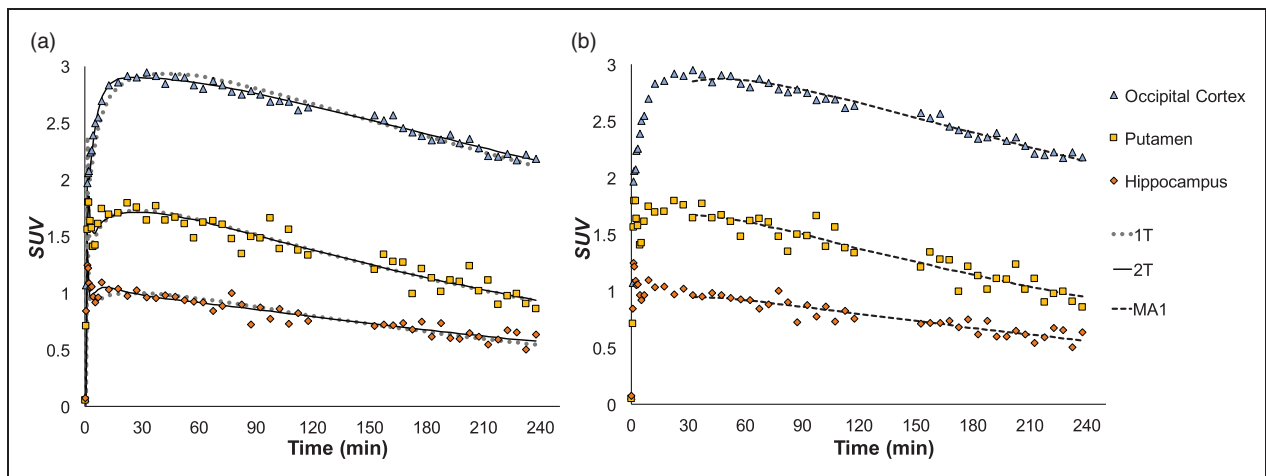


Figure 3. TACs and model fitting. (a) TACs from a representative participant's scan show high uptake with subsequent washout. 2T model (solid black line) had a superior visual fit compared to 1T (gray dotted line), particularly at early time points. (b) MA1 with $t^* = 30$ min (black dashed line) showing comparable fit to 2T.

Kinetic analysis

The optimal model configuration was a 2T model including estimation of F_V parameter. This model was selected by virtue of lowest AIC values with good visual fits in 85% of regions analyzed. Estimates of F_V ranged from 0.019 ± 0.006 in centrum semiovale to 0.057 ± 0.020 in cerebellum, K_1 ranged from 0.019 ± 0.006 mL/min/cm 3 in centrum semiovale to 0.066 ± 0.033 mL/min/cm 3 in occipital cortex, while estimates of V_T ranged from 3.2 ± 1.0 mL/cm 3 in centrum semiovale and caudate to 15.9 ± 4.2 mL/cm 3 in occipital cortex (all regions in Table 1).

Figure 3(a) shows 1T and 2T model fits to TACs from a representative participant. Although 1T did

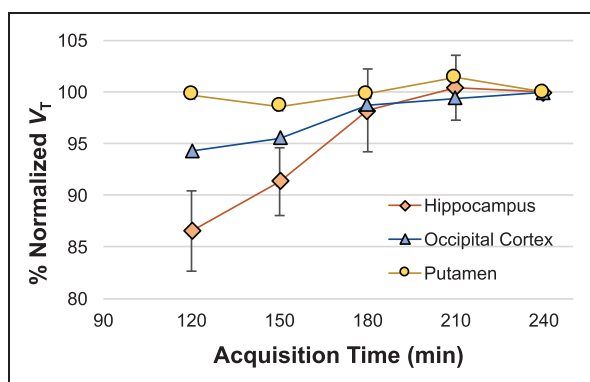
not describe the PET data as well as 2T, V_T estimates across regions agreed very well between the two approaches ($R^2 = 0.984$) (Supplementary Figure 1(a) and (b)).

The 2T model with fitted F_V in some cases produced unstable fits to TACs. Thus, the MA1 approach was also assessed (see Figure 3(b)). Using $t^* = 30$ min provided the best combination of high quality of quantitative fit and test–retest reliability. The MA1 method produced V_T estimates comparable to those stably estimated by 2T (Table 1) that were highly correlated ($R^2 = 0.990$; see Supplementary Figure 1(c) and (d)).

Truncation of acquired data revealed that V_T values estimated from 180 min of data using MA1 resulted in agreement within 5% of V_T estimated from 240 min of

Table 1. Values of F_V , K_1 (mL/min/cm³) for 2T and V_T (mL/cm³) for 2T and MA1 models at 180 min ($n = 12$, excluding unstable fits for 2T and corresponding fits for MA1).

Region	2T			MA1
	$F_V \pm$ S.D.	$K_1 \pm$ S.D.	$V_T \pm$ S.D.	$V_T \pm$ S.D.
Amygdala	0.043 \pm 0.010	0.027 \pm 0.005	3.9 \pm 1.6	3.7 \pm 1.6
Anterior cingulum	0.056 \pm 0.012	0.034 \pm 0.010	4.0 \pm 1.2	4.0 \pm 1.1
Caudate	0.031 \pm 0.016	0.045 \pm 0.023	3.2 \pm 1.0	3.2 \pm 1.0
Centrum semiovale	0.019 \pm 0.006	0.019 \pm 0.006	3.2 \pm 1.0	3.3 \pm 1.0
Cerebellum	0.057 \pm 0.020	0.057 \pm 0.023	12.6 \pm 5.5	12.5 \pm 5.4
Frontal cortex	0.055 \pm 0.014	0.048 \pm 0.014	8.5 \pm 2.2	8.5 \pm 2.2
Hippocampus	0.047 \pm 0.013	0.033 \pm 0.014	3.8 \pm 1.2	3.8 \pm 1.2
Insula	0.045 \pm 0.013	0.046 \pm 0.019	5.8 \pm 1.6	5.7 \pm 1.6
Occipital cortex	0.055 \pm 0.017	0.066 \pm 0.033	15.9 \pm 4.2	15.7 \pm 4.2
Parietal cortex	0.053 \pm 0.012	0.051 \pm 0.014	11.8 \pm 3.1	11.8 \pm 2.9
Putamen	0.041 \pm 0.014	0.056 \pm 0.028	8.1 \pm 3.2	8.0 \pm 2.9
Temporal cortex	0.052 \pm 0.011	0.046 \pm 0.014	9.1 \pm 3.5	8.7 \pm 2.5
Thalamus	0.045 \pm 0.009	0.050 \pm 0.012	13.4 \pm 5.6	13.1 \pm 5.7

**Figure 4.** Time stability of normalized V_T values. Time stability of MA1-estimated V_T values was evaluated using V_T estimated from truncated scan length normalized to V_T estimated from 240 min of imaging data. Mean percent normalized V_T values across scans ($n = 8$) are shown for representative brain regions.

imaging data for all regions except the amygdala (10% difference). Inter-individual standard deviation of time stability was $<10\%$ in all regions except for amygdala (18%) (Figure 4). Hence, 180 min of imaging data were used for subsequent characterization of test–retest variability.

Table 2 lists test–retest reliability data for V_T estimated with MA1 for four test–retest participants. Median absolute test–retest variability for MA1 was $16 \pm 5\%$ across regions of interest. Although the within-subject variability was higher than desirable, the ICC values were high, ranging from 0.67 to 0.97 for MA1 for all regions.

Table 2. Test–retest reliability of V_T values estimated using MA1 ($n = 4$).

Region	MA1		
	TRV (%)	aTRV (%)	ICC
Amygdala	13.3	13.3	0.97
Anterior cingulum	3.7	17.9	0.88
Caudate	−7.0	13.4	0.94
Centrum semiovale	2.1	17.2	0.87
Cerebellum	−10.7	23.9	0.92
Frontal cortex	0.6	14.0	0.93
Hippocampus	1.3	16.2	0.93
insula	2.3	10.0	0.95
Occipital cortex	0.6	16.6	0.89
Parietal cortex	9.9	27.4	0.67
Putamen	4.2	12.7	0.97
Temporal cortex	4.3	15.6	0.89
Thalamus	−2.9	23.4	0.88

ICC: intraclass correlation coefficient; TRV: test–retest variability.

Voxel-wise parametric images of [¹⁸F]AS2471907 V_T were generated with 1T due to noisy voxel-level data with MA1 estimation and excellent agreement in ROI-based V_T estimation between 1T and 2T (Supplementary Figure 1(a)). Voxel-wise V_T estimates showed regional patterns of availability similar to ROI-based estimates of V_T , and differences between test and retest voxel-wise images were visually consistent with TRV values observed for availability estimated by

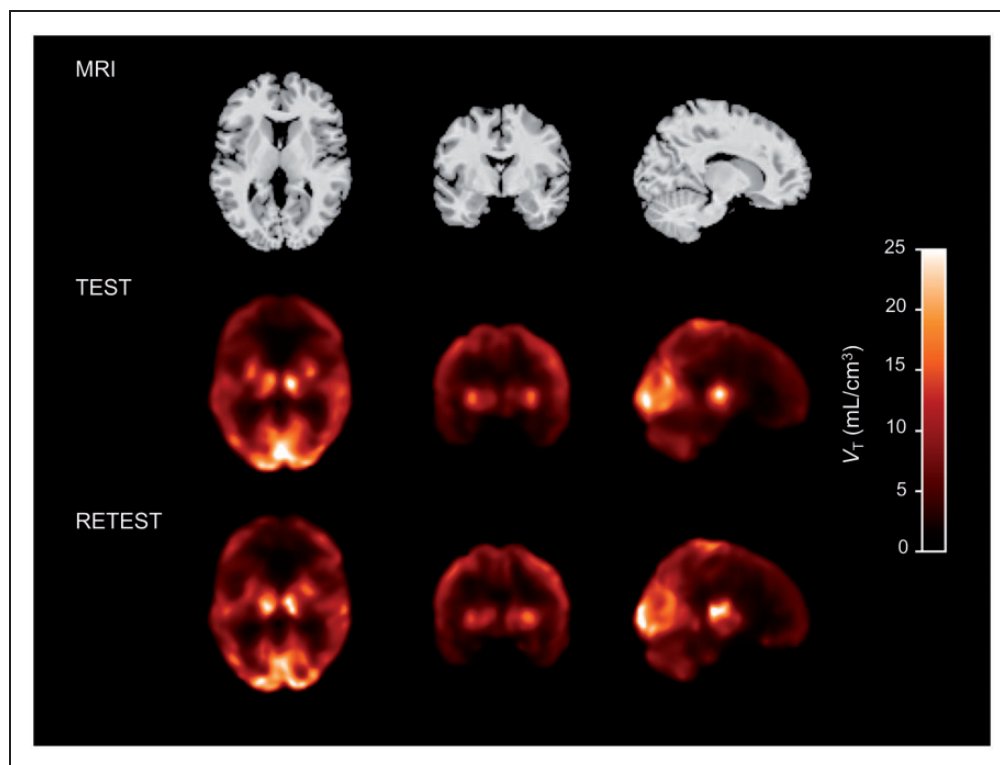


Figure 5. Parametric V_T images for test and retest scans. A representative participant's MRI (top) with co-registered test (middle) and retest (bottom) V_T images, where V_T is estimated from 180 min of imaging data using IT model with F_V fixed to 5%, smoothed with a 7mm Gaussian kernel.

ROI-based modeling (representative participant in Figure 5). Intra-regional heterogeneity was visibly apparent in voxel-wise [^{18}F]AS2471907 availability in areas corresponding to larger atlas-defined ROIs such as frontal cortex, parietal cortex, and cerebellum.

Average SUV values from 90 to 120 min ($R^2=0.814$), 120 to 150 min ($R^2=0.836$), and from 150 to 180 min ($R^2=0.851$) were correlated with V_T values estimated with MA1 from 180 min of data (Supplementary Figure 2).

Peripheral cortisol analysis

No significant relationships were observed between AUC of cortisol with whole-brain V_T and slope of cortisol decline (Supplementary Figure 3). Absolute test–retest variability for AUC of cortisol was under 20% for all but one participant in whom this value was 129%. The higher cortisol $aTRV$ values did not correspond to particularly high $aTRV$ of V_T in this individual.

Discussion

Here, we described the first in-human brain imaging evaluation of [^{18}F]AS2471907, a PET radiotracer

targeting 11 β -HSD1, in eight participants. A full kinetic characterization and assessment of time stability and test–retest reliability of primary outcome measures was performed.

Radioactivity in blood cleared quickly after a sharp increase in the first 5 min. Evaluation of metabolites of [^{18}F]AS2471907 demonstrated high parent fractions of approximately 70% after 240 min across test–retest participants. Radiometabolites were more polar than the parent compound, and therefore unlikely to enter the brain. The excellent time stability of V_T estimates is further consistent with negligible effects of brain-penetrant radiometabolites on the imaging data, as radiometabolites entering the brain could cause an apparent increase in V_T with longer scan lengths. The very low f_p values ($\sim 0.6\%$) make V_T/f_p an unsuitable outcome measure for this radiotracer.

[^{18}F]AS2471907 displayed highest radioactivity uptake in thalamus, cerebellum, and cortical regions, particularly occipital cortex. Moderate uptake was seen in frontal, parietal, temporal cortices, and insula as well as in putamen and midbrain regions. Lower uptake was observed in most subcortical brain regions, including limbic brain regions of amygdala and hippocampus, with very little uptake in white matter. The higher uptake in later peaking regions compared

to striatal and limbic regions and white matter was similar to the distribution of [^{11}C]AS2471907 in human.¹⁵ Regional [^{18}F]AS2471907 V_T values were well correlated with regional 11 β -HSD1 mRNA expression from the Allen Human Brain Atlas^{15,29} (probes 1027298 and 1027299) in gray matter regions ($R^2=0.676$, $p < 0.003$, $n = 12$), with even stronger correlation in cortical regions ($R^2=0.872$, $p < 0.02$, $n = 5$). Values of V_T were low in hippocampus, which is consistent with the approximately four-fold lower 11 β -HSD1 enzyme activity in hippocampus relative to cerebellum previously reported in humans.¹³ As 11 β -HSD1 enzyme activity across other human brain regions has not been reported, a current limitation of this work is the inability to compare regional [^{18}F]AS2471907 V_T values to 11 β -HSD1 enzyme activity outside of hippocampus and cerebellum.

Analysis of time-activity curves with 1T and 2T compartment models revealed that 2T with an estimated vascular fraction (F_v) best described radiotracer behavior in gray matter regions. The importance of modeling the vascular fraction is consistent with the low K_1 estimates of 0.02–0.07 mL/min/cm³ (Table 1), indicative of a low extraction fraction for [^{18}F]AS2471907 likely due, at least in part, to the very low f_p . However, some 2T analyses did not converge or resulted in implausible V_T estimates, which prompted implementation of MA1 to estimate V_T . MA1 with $t^* = 30$ min yielded V_T estimates that were highly correlated with those of 2T. Based on the robust estimation of V_T by MA1 and computational efficiency, MA1 with $t^* = 30$ min is the recommended method for regional V_T estimation of [^{18}F]AS2471907 imaging data.

Regional heterogeneity in [^{18}F]AS2471907 uptake was visually apparent in late SUV images, motivating the desire to create voxel-wise parametric images. These images were generated with 1T, despite the additional computational complexity, due to the excellent agreement of regional V_T estimates with estimates by 2T and the improved robustness to noisy voxel data, particularly for voxels with high V_T ,³⁰ relative to MA1 and Logan graphical analyses.³¹ These voxel-wise parametric maps confirmed significant within-(atlas-defined) region heterogeneity in V_T (see Figure 5). For example, the midline cerebellum, sensorimotor cortical areas, and lateral thalamic areas consistently exhibited higher [^{18}F]AS2471907 availability than other areas of their respective atlas-defined regions, echoing previously reported ‘patchy microdistribution’ of 11 β -HSD1 expression and activity in rodent brain.^{32,33} Interestingly, these regions are known to have highest expression of *11bHSD1* gene in rat brain, but in a heterogeneous pattern with particularly high expression in Purkinje cells of cerebellum, and layer IV neurons of parietal cortex and caudal areas of frontal cortex.³²

This within-region heterogeneity may be an important consideration for MRI atlas-based ROI approaches, which implicitly average the uptake within regions.

Simplified quantification approaches were explored to reduce the logistical complication of arterial blood sampling. Blocking studies of [^{18}F]AS2471907 in non-human primate¹⁶ and of the ^{11}C -labeled analog [^{11}C]AS2471907 in humans demonstrated that nearly all brain radioactivity uptake was specifically bound,¹⁵ thus precluding the use of reference region approaches for this target. SUV values were considered as a candidate semi-quantitative approach for this radiotracer owing to the excellent inter- and intra-subject consistency of the arterial input function (see Figure 2(b)) and near-complete blockade of uptake in brain, indicating that the tissue curves represent nearly all specific signals. SUV values measured at 150–180 min post-injection provided good agreement with V_T estimates ($R^2=0.851$). Test-retest reliability of SUV was also comparable to that of V_T estimates, with $aTRV$ ranging from 11 to 18% for SUV averaged over 90–120 min, 12–19% for 120–150 min, and 13–19% for 150–180 min. However, tissue-to-plasma activity ratios (TTP) at 150–180 min across regions were not as well correlated with V_T with $R^2=0.706$ ($n = 12$) and continued to increase throughout the imaging period, indicating that transient equilibrium was not yet achieved. Thus, while SUV provides a simplified quantification approach, it remains susceptible to individual differences in [^{18}F]AS2471907 influx or clearance and would therefore require careful validation in a study population.

Quantification of [^{18}F]AS2471907 V_T exhibited modest test-retest variability ($aTRV$) and good intra-subject reliability (ICC) for MA1 method. The high ICC values are explained by the large between-subject variability, with regional coefficients of variation (CoV) ranging from 25 to 43%. V_T values were globally higher on test than retest day for two male participants and globally lower for the female participant, suggesting that intra-individual variability in V_T may be state dependent. Although daily cortisol output and rate of decline in afternoon cortisol have both been found to be related to HPA axis dysregulation,^{27,28} plasma cortisol levels did not appear to explain variability in whole brain [^{18}F]AS2471907 V_T within or across these subjects (Supplementary Figure 3). Exploratory post-hoc analyses across all ROIs did not reveal any regionally significant relationships. Moreover, all scans were acquired at the same time of day to minimize the possibility of diurnal cortisol levels influencing [^{18}F]AS2471907 V_T . Future work is required to determine whether brain cortisol levels modulate [^{18}F]AS2471907 kinetics. Given the large between-subject variability which would limit statistical power to

detect group differences, the extent to which between-subject variability can be explained by biological variables such as brain cortisol levels, BMI,³⁴ or other factors remains a critical outstanding question for future use of this radiotracer.

[¹⁸F]AS2471907 was developed from the [¹¹C]AS2471907 compound, with the dual goals of improved efficiency for routine production and improved quantification from increased counting statistics afforded by the ¹⁸F-label. The magnitude and pattern of regional V_T values were comparable between both radiotracers. In addition, the large between-subject variability (CoVs~30–40%) and modest test–retest variability (<20%) were comparable between both radiotracers.¹⁵ While fluorine-18 labeling of AS2471907 provided only marginal improvement in quantification properties over the carbon-11-labeled version, the improved efficiency and reliability in the radiosynthesis of [¹⁸F]AS2471907 yield important practical advantages for future use of [¹⁸F]AS2471907 to image 11 β -HSD1 in human brain.

In conclusion, [¹⁸F]AS2471907 exhibits suitable kinetic properties for quantification of 11 β -HSD1 in human brain. Based on the substantial between-subject variability, this radiotracer may have limited statistical power to detect between-group differences in 11 β -HSD1 levels. Future work is therefore needed to characterize whether identifiable biological factors contribute to this variability. Nonetheless, this radiotracer holds potential for future study of 11 β -HSD1 in neuropsychiatric, metabolic, and inflammatory conditions.

Funding

The author(s) disclosed receipt of the following financial support for the research, authorship, and/or publication of this article: the Office of Research on Women's Health, Brain and Behavior Foundation NARSAD Young Investigator Grant, Veterans Affairs National Center for PTSD, Gustavus and Louise Pfeiffer Foundation, and the following NIH Grants: P50DA033945; K02DA03175; K01AA024788; T32GM007205; F30MH116607; R56MH116941.

Acknowledgements

We thank the staff at the Yale PET center for their expertise and support of radiochemistry and imaging.

Declaration of conflicting interests

The author(s) declared no potential conflicts of interest with respect to the research, authorship, and/or publication of this article.

Authors' contributions

SB and ATH performed imaging analysis and wrote the article. NBN, SL, ZC and YH developed and optimized radiosynthesis methods for [¹⁸F]AS2471907. DM was the study

physician. JB conducted analysis of 11 β -HSD1 mRNA data from Allen Brain Atlas. NN, SN, and JRP synthesized [¹⁸F]AS2471907 on PET imaging days. MK conducted radio-metabolite analysis. SB, ATH, KPC, REC, and YH determined imaging conditions and study design. All authors edited the article.

ORCID iD

Shivani Bhatt  <http://orcid.org/0000-0003-3494-7246>

Supplemental material

Supplemental material for this paper can be found at the journal website: <http://journals.sagepub.com/home/jcb>

References

- Herman JP, Ostrander MM, Mueller NK, et al. Limbic system mechanisms of stress regulation: hypothalamo-pituitary-adrenocortical axis. *Progr Neuro-Psychopharmacol Biol Psychiatry* 2005; 29: 1201–1213.
- Yehuda R, Teicher MH, Trestman RL, et al. Cortisol regulation in posttraumatic stress disorder and major depression: A chronobiological analysis. *Biol Psychiatry* 1996; 40: 79–88.
- Yehuda R. Post-traumatic stress disorder. *N Engl J Med* 2002; 346: 108–114.
- Morris MC, Compas BE and Garber J. Relations among posttraumatic stress disorder, comorbid major depression, and HPA function: a systematic review and meta-analysis. *Clin Psychol Rev* 2012; 32: 301–315.
- Chao AM, Jastreboff AM, White MA, et al. Stress, cortisol, and other appetite-related hormones: prospective prediction of 6-month changes in food cravings and weight. *Obesity* 2017; 25: 713–720.
- Jackson SE, Kirschbaum C and Steptoe A. Hair cortisol and adiposity in a population-based sample of 2,527 men and women aged 54 to 87 years. *Obesity* 2017; 25: 539–544.
- Chapman K, Holmes M and Seckl J. 11beta-hydroxysteroid dehydrogenases: intracellular gate-keepers of tissue glucocorticoid action. *Physiol Rev* 2013; 93: 1139–1206.
- Meijer OC, Karssen AM and de Kloet ER. Cell- and tissue-specific effects of corticosteroids in relation to glucocorticoid resistance: examples from the brain. *J Endocrinol* 2003; 178: 13–18.
- Yau JLW, Noble J and Seckl JR. 11 β -Hydroxysteroid dehydrogenase type 1 deficiency prevents memory deficits with aging by switching from glucocorticoid receptor to mineralocorticoid receptor-mediated cognitive control. *J Neurosci* 2011; 31: 4188.
- Yau Joyce LW, Noble J, Kenyon Christopher J, et al. Diurnal and stress-induced intra-hippocampal corticosterone rise attenuated in 11 β -HSD1-deficient mice: a microdialysis study in young and aged mice. *Eur J Neurosci* 2015; 41: 787–792.
- Sarabdjitsingh RA, Zhou M, Yau JL, et al. Inhibiting 11beta-hydroxysteroid dehydrogenase type 1 prevents

- stress effects on hippocampal synaptic plasticity and impairs contextual fear conditioning. *Neuropharmacology* 2014; 81: 231–236.
12. Webster SP, McBride A, Binnie M, et al. Selection and early clinical evaluation of the brain-penetrant 11 β -hydroxysteroid dehydrogenase type 1 (11 β -HSD1) inhibitor UE2343 (XanamemTM). *Br J Pharmacol* 2016; 174: 396–408.
 13. Sandeep TC, Yau JLW, MacLulich AMJ, et al. 11 β -Hydroxysteroid dehydrogenase inhibition improves cognitive function in healthy elderly men and type 2 diabetics. *Proc Natl Acad Sci USA* 2004; 101: 6734.
 14. Boyle CD and Kowalski TJ. 11 β -hydroxysteroid dehydrogenase type 1 inhibitors: a review of recent patents. *Expert Opin Ther Patents* 2009; 19: 801–825.
 15. Gallezot J-D, Nabulsi N, Henry S, et al. Imaging the enzyme 11beta-hydroxysteroid dehydrogenase type 1 with positron emission tomography: evaluation of the novel radiotracer [(11)C]AS2471907 in human brain. *J Nucl Med* (in press).
 16. Baum E, Zhang W, Li S, et al. A novel 18F-labeled radioligand for positron emission tomography imaging of 11 β -hydroxysteroid dehydrogenase (11 β -HSD1): synthesis and preliminary evaluation in nonhuman primates. *ACS Chem Neuroscience*. Epub ahead of print 28 February 2019. DOI: 10.1021/acchemneuro.8b00715.
 17. Désir D, Van Cauter E, Golstein J, et al. Circadian and ultradian variations of ACTH and cortisol secretion. *Hormones* 1980; 13: 302–316.
 18. Carson RE, Barker WC, Liow J-S, et al. Design of a motion-corrected OSEM list-mode algorithm for resolution-recovery reconstruction for the HRRT. *IEEE Nucl Sci Symp Conf Rec* 2003; 5: 3281–3285.
 19. Hilton J, Yokoi F, Dannals RF, et al. Column-switching HPLC for the analysis of plasma in PET imaging studies. *Nucl Med Biol* 2000; 27: 627–630.
 20. Tzourio-Mazoyer N, Landeau B, Papathanassiou D, et al. Automated anatomical labeling of activations in SPM using a macroscopic anatomical parcellation of the MNI MRI single-subject brain. *NeuroImage* 2002; 15: 273–289.
 21. Innis RB, Cunningham VJ, Delforge J, et al. Consensus nomenclature for in vivo imaging of reversibly binding radioligands. *J Cereb Blood Flow Metab* 2007; 27: 1533–1539.
 22. Schmidt KC and Turkheimer. Kinetic modeling in positron emission tomography. *Q J Nucl Med* 2002; 46: 70–85.
 23. Leenders KL, Perani D, Lammertsma AA, et al. Cerebral blood flow, blood volume and oxygen utilization normal values and effect of age. *Brain* 1990; 113: 27–47.
 24. Watabe H, Channing MA, Der MG, et al. Kinetic analysis of the 5-HT_{2A} ligand [11C]MDL 100,907. *J Cereb Blood Flow Metab* 2000; 20: 899–909.
 25. Ichise M, Toyama H, Innis RB, et al. Strategies to improve neuroreceptor parameter estimation by linear regression analysis. *J Cereb Blood Flow Metab* 2002; 22: 1271–1281.
 26. Bremner JD, Vythilingam M, Vermetten E, et al. Cortisol response to a cognitive stress challenge in posttraumatic stress disorder (PTSD) related to childhood abuse. *Psychoneuroendocrinology* 2003; 28: 733–750.
 27. Stone AA, Schwartz JE, Smyth J, et al. Individual differences in the diurnal cycle of salivary free cortisol: a replication of flattened cycles for some individuals. *Psychoneuroendocrinology* 2001; 26: 295–306.
 28. Tucker P, Beebe KL, Burgin C, et al. Paroxetine treatment of depression with posttraumatic stress disorder: effects on autonomic reactivity and cortisol secretion. *J Clin Psychopharmacol* 2004; 24: 131–140.
 29. Hawrylycz MJ, Lein ES, Guillozet-Bongaarts AL, et al. An anatomically comprehensive atlas of the adult human brain transcriptome. *Nature* 2012; 489: 391.
 30. Slifstein M and Laruelle M. Effects of statistical noise on graphic analysis of PET neuroreceptor studies. *J Nucl Med* 2000; 41: 2083–2038.
 31. Logan J, Fowler JS, Volkow ND, et al. Graphical analysis of reversible radioligand binding from time–activity measurements applied to [N-11C-Methyl]-(-)-cocaine PET studies in human subjects. *J Cereb Blood Flow Metab* 1990; 10: 740–747.
 32. Moisan M-P, Seckl JR and Edwards CRW. 11 β -hydroxysteroid dehydrogenase bioactivity and messenger rna expression in rat forebrain: localization in hypothalamus, hippocampus, and cortex. *Endocrinology* 1990; 127: 1450–1455.
 33. Wyrwoll CS, Holmes MC and Seckl JR. 11 β -hydroxysteroid dehydrogenases and the brain: from zero to hero, a decade of progress. *Front Neuroendocrinol* 2011; 32: 265–286.
 34. Bini J, Jastreboff A, Gallezot J-D, et al. Reduction of 11 β -hydroxysteroid dehydrogenase type 1 enzyme levels with increasing body mass index: a Brain PET imaging study. *J Nucl Med* 2018; 59: 1300.